sustainability

MDPI

Article

Two-Step Hydrothermal Reaction Enhances Removal of Cr(VI) from Wastewater Using Nitrogen-Doped Starch-Based Hydrothermal Carbon

Borui Zhang, Xinyu Wan, Chenghong Li, Kaiyue Ma, Xinyu Wu, Hongxu Liang and Hongxiang Hu *

College of Resources and Environment, Anhui Agricultural University, Hefei 230036, China; zhangborui@ahau.edu.cn (B.Z.); 23720694@stu.ahau.edu.cn (X.W.); lch0792@stu.ahau.edu.cn (C.L.); wuxinyu0511@stu.ahau.edu.cn (X.W.); lianghongxu@ahau.edu.cn (H.L.)
* Correspondence: hongxianghu@ahau.edu.cn

Abstract: Extracting Cr(VI), a heavy metal known for its carcinogenic properties, from water poses a significant challenge. This research involved synthesizing nitrogen-infused starch-derived hydrothermal carbon (NS-HCS) from starch using a dual-phase hydrothermal method, aimed at removing Cr(VI) from industrial wastewater. N-doping increased the N content from 0.27% to 3.64%, providing active sites for enhanced Cr(VI) adsorption and reduction. Experimental data demonstrated 149.21 mg/g contaminant uptake capacity with 49.74% removal efficiency under specified conditions. Analysis of the kinetic and isotherm models revealed that the adsorption mechanism was characterized primarily by multilayer adsorption. Furthermore, after six cycles of use, NS-HCS demonstrated good reusability, with its Cr(VI) adsorption capacity remaining at approximately 79.05%. Additionally, NS-HCS exhibited strong resistance to interference in complex aqueous environments. This study provides new insights into the use of green and sustainable adsorbents, offering an economical and efficient solution for treating Cr(VI)-contaminated wastewater.

Keywords: starch-based hydrothermal carbon; nitrogen doping; Cr(VI) removal; adsorption performance; regeneration

Received: 11 April 2025
Revised: 11 May 2025
Accepted: 26 May 2025
Published: 29 May 2025

Citation: Zhang, B.; Wan, X.; Li, C.; Ma, K.; Wu, X.; Liang, H.; Hu, H. Two-Step Hydrothermal Reaction Enhances Removal of Cr(VI) from Wastewater Using Nitrogen-Doped Starch-Based Hydrothermal Carbon. *Sustainability* **2025**, *17*, 4982. https://doi.org/10.3390/su17114982

1. Introduction

Accelerated industrial growth and urban development have drastically intensified metallic pollutant release into hydrological systems, creating severe ecological and public health hazards. These heavy metal pollutants primarily originate from various industrial activities, such as mining, leather processing, textile manufacturing, electroplating, and metal processing [1–3]. Compared to other industrial wastewater sources, electroplating effluent shows substantially elevated Cr(VI) concentrations [4–7], even exceeding Chinese discharge standards by tens of thousands of times [8,9]. Aquatic Cr(VI) speciation primarily involves trivalent and hexavalent states, the latter demonstrating extreme toxicity through teratogenic, carcinogenic, and mutagenic effects. Cr(VI) compounds exhibit exceptional hydrophilicity and environmental mobility, enabling trophic transfer and eventual human ingestion pathways [10–13]. Therefore, it is critically important to conduct thorough research on the treatment of Cr(VI)-contaminated wastewater.

Presently, various techniques are employed to remove Cr(VI) from water [14–17]. Among these, adsorption stands out due to its wide usage. Traditional adsorbents have limited adsorption capacity, are expensive, and are nonrenewable [18–20]. To achieve environmentally friendly, efficient, and economical removal effects, there is an increasing

demand for new, cost-effective, and ecofriendly adsorbents. Carbon materials have become a research hotspot in recent years. Hydrothermal carbons—a biochar derivative—enhance sorptive performance through surface oxygen group augmentation [21–24]. Starch, as a high-quality biomass, is widely available, low-cost, and easy to process. Therefore, converting starch into hydrothermal carbon through hydrothermal treatment to improve its adsorption performance is a viable solution [25–27].

The single hydrothermal treatment of carbon materials is still insufficient for treating high-concentration Cr(VI) wastewater [15,28]. The presence of these nitrogen-based functional groups enhances the surface behavior of carbon and improves its absorption capacity [29–32]. Therefore, preparing nitrogen-doped hydrothermal carbon from starch through a two-step hydrothermal process, which combines oxygen and nitrogen active sites, is expected to efficiently treat Cr(VI)-contaminated wastewater.

This research involved the creation of nitrogen-infused starch-derived hydrothermal carbon (NS-HCS) from starch through a dual-stage hydrothermal process. Structural characterization incorporated electron microscopy imaging coupled with multiple spectroscopic analyses. Systematic batch experiments evaluated pH dependence, temporal adsorption patterns, and thermal influences on Cr(VI) sequestration performance. Experiments involving regeneration and competitive adsorption were conducted to assess the reusability and resistance of NS-HCS to interference. Various kinetic and isotherm models were employed to examine the adsorption properties of NS-HCS for Cr(VI). The developed material demonstrates cost-effective production, ecological compatibility, and scalable implementation potential for Cr(VI)-laden wastewater purification applications.

2. Materials and Methods

2.1. Materials

National Pharmaceutical Group Chemical Reagent Co., Ltd. supplied the starch and urea utilized in this study (Hefei, China).

2.2. Synthesis of Starch-Based Two-Step Hydrothermal Carbon

A total of 15 g of starch underwent homogenization with 150 mL ultrapure water through continuous agitation. This suspension was loaded into a 250 mL hydrothermal vessel for carbonization under 200 °C thermal treatment lasting 360 min, with mechanical rotation sustained at 500 rpm. Post-reaction separation employed 0.22 μm microfiltration membranes, succeeded by triple rinsing cycles using 95% ethanol and ultrapure water. Resultant precipitates were thermally dehydrated in 60–80 °C drying chambers over 6 h to yield starch-derived hydrothermal carbonaceous substrates (SHCSs).

In the subsequent phase, 3 g of the SHCS and urea each were mixed into 150 mL of ultrapure water and agitated until a consistent mixture was achieved. The blend was then transferred to hydrothermal reactor and exposed to identical hydrothermal conditions as the initial phase. The final product, nitrogen-doped starch-based hydrothermal carbon (NS-HCS), was obtained after filtration, washing, and drying.

2.3. Characterization of Hydrothermal Carbon

The synthesized SHCS and NS-HCS were characterized using various physicochemical methods. Elemental analysis was performed using an Elementar UNICUBE (Germany). Zeta potential measurements were conducted with a Malvern Zetasizer Pro instrument (UK). Molecular vibration profiling occurred through Japanese IRTracer 100 Fourier-transform infrared spectrometers. Chemical state analyses implemented American K-Alpha X-ray photoelectron spectrometers. Morphological examinations leveraged German-

origin sigma500 scanning electron microscopes (All the instruments were purchased in Hefei, China).

2.4. Adsorption Experiments

Cr(VI) solutions were synthesized from potassium dichromate precursors. Precisely measured 0.4 g/L NS-HCS quantities were introduced into 100 mL centrifugal containers, subsequently charged with 50 mL Cr(VI) solutions. The pH regulation occurred through 0.1 mol/L HCl and NaOH titrations. Reaction vessels underwent thermo-regulated orbital agitation at specified oscillation frequencies. Post-equilibrium suspensions underwent 0.22 μm membrane filtration, with residual Cr(VI) concentrations analyzed via ultraviolet-visible spectroscopy. The research investigated how the pH of the solution, the initial concentration of Cr(VI), the length of adsorption, and temperature influence its adsorption capacity. Experiments involving kinetics, isotherm modeling (Supplementary Materials), competitive ion modeling, and regeneration were also conducted. The equilibrium adsorption quantity was calculated using the following expression:

$$q_e = \frac{(\rho_1 - \rho_2)V}{m} \quad (1)$$

In the mathematical expression, q_e represents equilibrium adsorption capacity (mg/g), ρ_1 denotes initial solute concentration (mg/L), ρ_2 signifies equilibrium solute concentration (mg/L), V corresponds to solution volume (L), and m indicates adsorbent quantity (g).

2.5. Adsorption Regeneration

NS-HCS reusability underwent evaluation across six sequential adsorption–regeneration cycles under the following standardized parameters: 0.4 g/L material loading, 50 mg/L initial Cr(VI) concentration, pH 2.0 environment, 25 °C ambient temperature, and 24 h equilibrium period with constant agitation. Post-sorption suspensions underwent filtration via 0.22 μm hydrophilic membranes. Retrieved adsorbents underwent 60 °C thermal dehydration for four hours prior to alkaline elution using 1 M NaOH (24 h immersion). The regenerated NS-HCS was re-filtered (0.22 μm), dried (60 °C, 4 h), and reused for subsequent cycles.

3. Results and Discussion

3.1. Microstructure and Elemental Distribution

3.1.1. Surface Morphology

The morphological characterization of starch-derived hydrothermal carbon spheres (SHCSs) and nitrogen-enriched counterparts (NS-HCS) utilized scanning electron microscopy (SEM) for a comprehensive structural evaluation. High-resolution imaging revealed significant architectural modifications in starch morphology during hydrothermal carbonization processing. The primary product of the first hydrothermal step, SHCSs, exhibited a spherical structure with sizes ranging from submicron to several microns (Figure 1a,b). The surface of these carbon spheres appeared relatively smooth, indicating a homogeneous nucleation process during hydrothermal synthesis. This smooth surface morphology suggests that the reaction conditions were consistent throughout the process, leading to uniform carbon sphere formation.

Upon closer inspection (Figure 1c), it was observed that the carbon spheres had a slightly roughened surface, which could be attributed to the inherent texture of the carbonized starch. The size variation among the spheres is likely due to differences in the hydrolysis rates of the starch during the carbonization process. Spheres that formed earlier had more time to grow, resulting in larger diameters, while those that nucleated

later remained smaller. This phenomenon is consistent with the behavior of glucose during hydrothermal carbonization, as starch is a polymer of glucose.

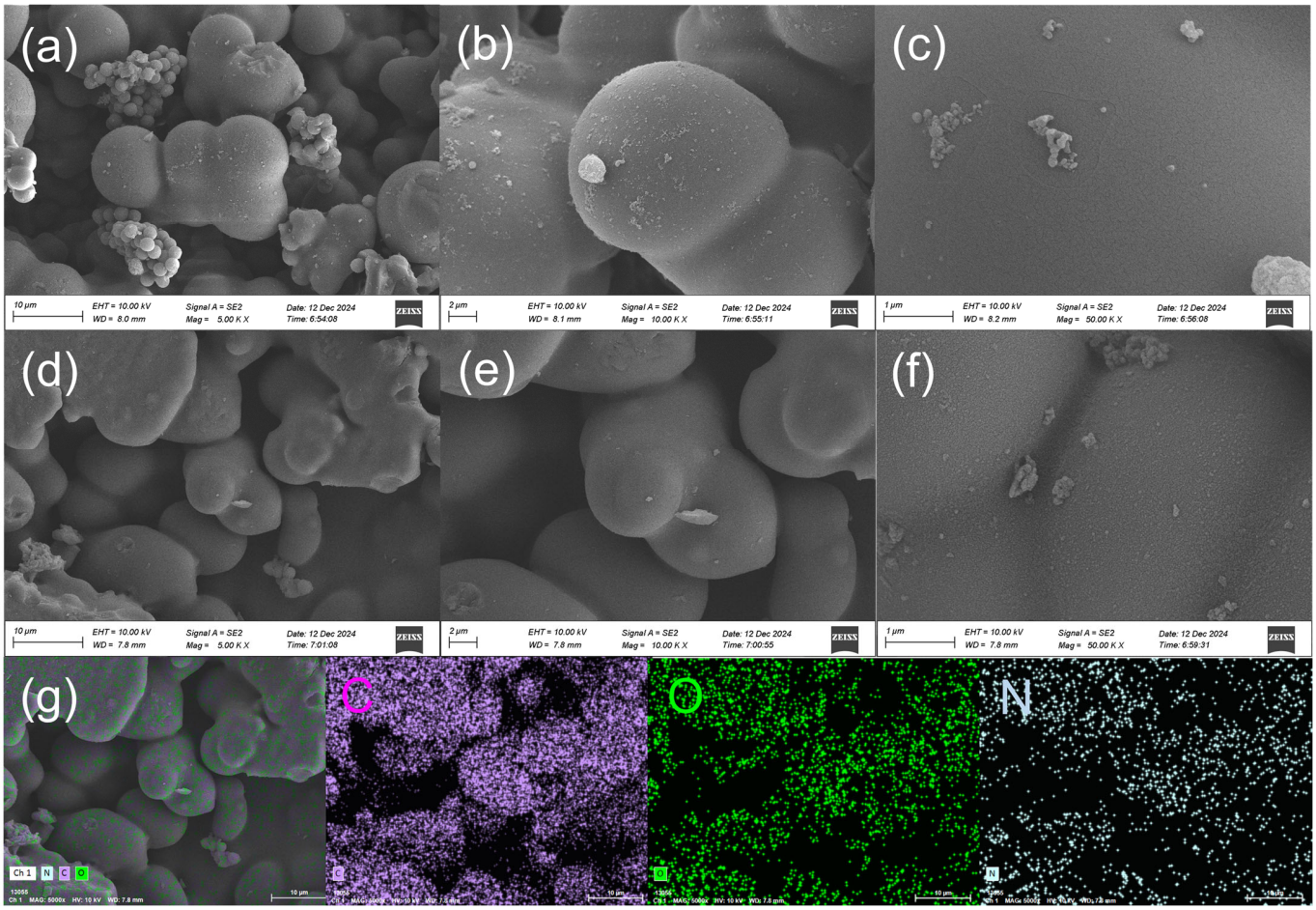

Figure 1. Surface morphology and elemental distribution of S-HCS and NS-HCS: (**a**–**c**) SEM images of S-HCS; (**d**–**f**) SEM images of NS-HCS; (**g**) SEM-EDS spectrum of NS-HCS.

In the second hydrothermal step, the introduction of urea led to the formation of NS-HCS. The SEM images of NS-HCS (Figure 1d,e) showed that the carbon spheres retained their spherical shape but exhibited a more irregular surface compared to SHCSs. This roughness is attributed to the deposition of nitrogen-containing compounds derived from the thermal decomposition of urea. Nitrogen doping not only altered the surface texture but also introduced new functional groups, improving the material's adsorption capabilities.

Elemental dispersion patterns across NS-HCS matrices underwent detailed spatial analysis through energy-dispersive X-ray spectroscopy (EDS) (Figure 1f). EDS mapping analysis revealed an even distribution of carbon (C), nitrogen (N), and oxygen (O) components across the NS-HCS surface. The presence of nitrogen confirmed the successful doping of urea-derived nitrogen into the carbon matrix, which is crucial for enhancing the adsorption capacity for Cr(VI).

3.1.2. Elemental Composition and Chemical Structure

The elemental makeup of the materials was ascertained using an organic elemental analyzer (Table 1). Findings showed carbon (C) as the primary component in both SHCSs and NS-HCS, constituting about 67–68% of the total. The hydrogen (H) and oxygen (O) contents were similar in both materials, with H accounting for 4.26% in SHCSs and 4.42% in NS-HCS and O accounting for 22.94% in SHCSs and 21.05% in NS-HCS. Elevated oxygen

levels in both substances suggested the presence of numerous oxygen-rich functional groups, which are beneficial for capturing and reducing Cr(VI) [18,33]. The nitrogen content increased from 0.27% in SHCSs to 3.64% in NS-HCS after the second hydrothermal step, confirming the successful incorporation of nitrogen from urea, which provides active sites conducive to Cr(VI) adsorption and reduction.

Table 1. Elemental composition of material.

Material	C (%)	H (%)	O (%)	N (%)
S-HCS	67.25	4.26	22.94	0.27
NS-HCS	68.31	4.42	21.05	3.64

The chemical composition analysis of SHCSs and NS-HCS employed Fourier-transform infrared spectroscopy (FT-IR) coupled with X-ray photoelectron spectroscopy (XPS). FT-IR absorption bands (Figure 2) identified characteristic oxygenated and carbonaceous functional moieties, including hydroxyl stretching (ν-OH), aliphatic C-H bonds, carbonyl groups (C=O), aromatic ring vibrations (ν-C=C), phenolic C-OH linkages, ether C-O-C bonds, and hydroxyl deformation modes (δ-OH). Secondary hydrothermal treatment-induced the attenuation of ν-OH, C-H, C=O, ν-C=C, and C-OH signatures, attributable to nitrogen incorporation. This structural modification's impact on sorptive performance was quantitatively assessed through concurrent XPS analysis.

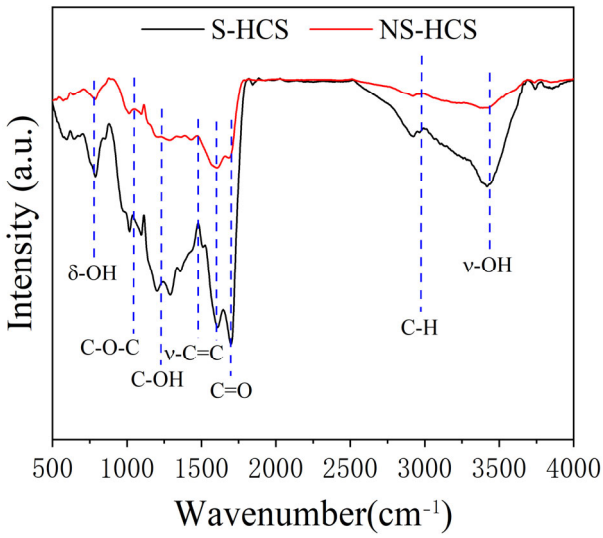

Figure 2. FTIR spectra of the materials.

XPS analysis revealed that the C1s and O1s peaks in NS-HCS were similar to those in SHCSs, while the N1s peak was more pronounced, consistent with the elemental analysis results (Figure 3a). Deconvoluted C1s spectra revealed three principal carbon states, namely C-C/C=C/CHx (284.57 eV), C-OR/C=N (285.62 eV), and -COOR (288.55 eV) (Figure 3b) [34–36]. O1s spectral resolution delineated two distinct oxygen states—C=O (531.82 eV) and -C-O- (533.20 eV) (Figure 3c) [35,36]. The N1s peak exhibited a characteristic peak for pyridinic-N (399.32 eV) (Figure 3d) [37]. Existing research correlates these functional motifs with enhanced Cr(VI) adsorption capacities through synergistic redox interactions, potentially explaining NS-HCS's superior performance [22].

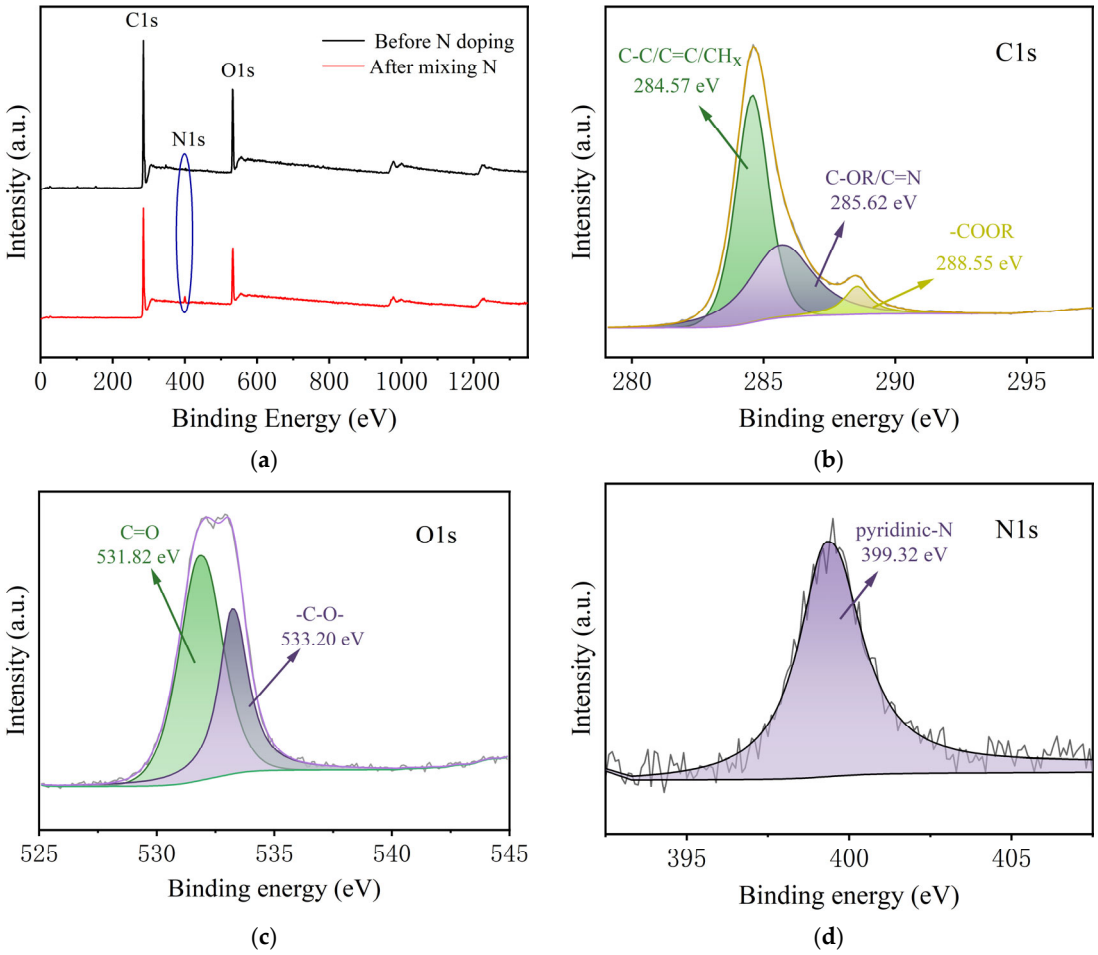

Figure 3. Compositional characterization of synthesized materials: (**a**) total XPS spectrum of the material; (**b**) C1s peak of NS-HCS; (**c**) O1s peak of NS-HCS; (**d**) N1s peak of NS-HCS.

3.2. Effects of Environmental Conditions on Cr(VI) Adsorption by NS-HCS

Surface electrochemical characteristics of NS-HCS exhibited pronounced pH dependency, with optimal Cr(VI) removal efficiency (149.21 mg/g) achieved at pH 2.0 (Figure 4a). This is because Cr(VI) primarily exists as $HCrO_4^-$ and $Cr_2O_7^{2-}$ ions within this pH range, and these ions show a strong attraction to the oxygen-rich functional groups on the NS-HCS surface, facilitating their removal from the solution [38,39]. Surface charge potential measurements corroborated Cr(VI) adsorption trends across pH gradients, revealing a point of zero charge at pH 3.4. Protonated surfaces below this threshold facilitated the electrostatic attraction of anionic Cr(VI) complexes, with intensified adsorption observed under progressively acidic conditions. Conversely, when the pH exceeded 3.4, the surface of NS-HCS carried a negative charge, leading to a weakened or repulsive adsorption of Cr(VI) ions.

Thermally modulated Cr(VI) adsorption behavior of NS-HCS revealed progressive capacity enhancement with rising thermal energy inputs, attributed to intensified molecular thermal agitation promoting adsorbate–adsorbent collisions [16]. Experiments were conducted at 298, 308, and 318 K, with a Cr(VI) concentration of 300 mg/L, to examine the effect of temperature on the adsorption capacity of NS-HCS. NS-HCS showed enhanced Cr(VI) adsorption capacity at elevated temperatures, achieving 149.21 mg/g at 318 K compared to 116.49 mg/g at 298 K. (Figure 4b). Comparative analysis against existing adsorbent technologies (Table 2) confirmed NS-HCS's superior Cr(VI) uptake capacities, highlighting its temperature-responsive performance advantages [40–43].

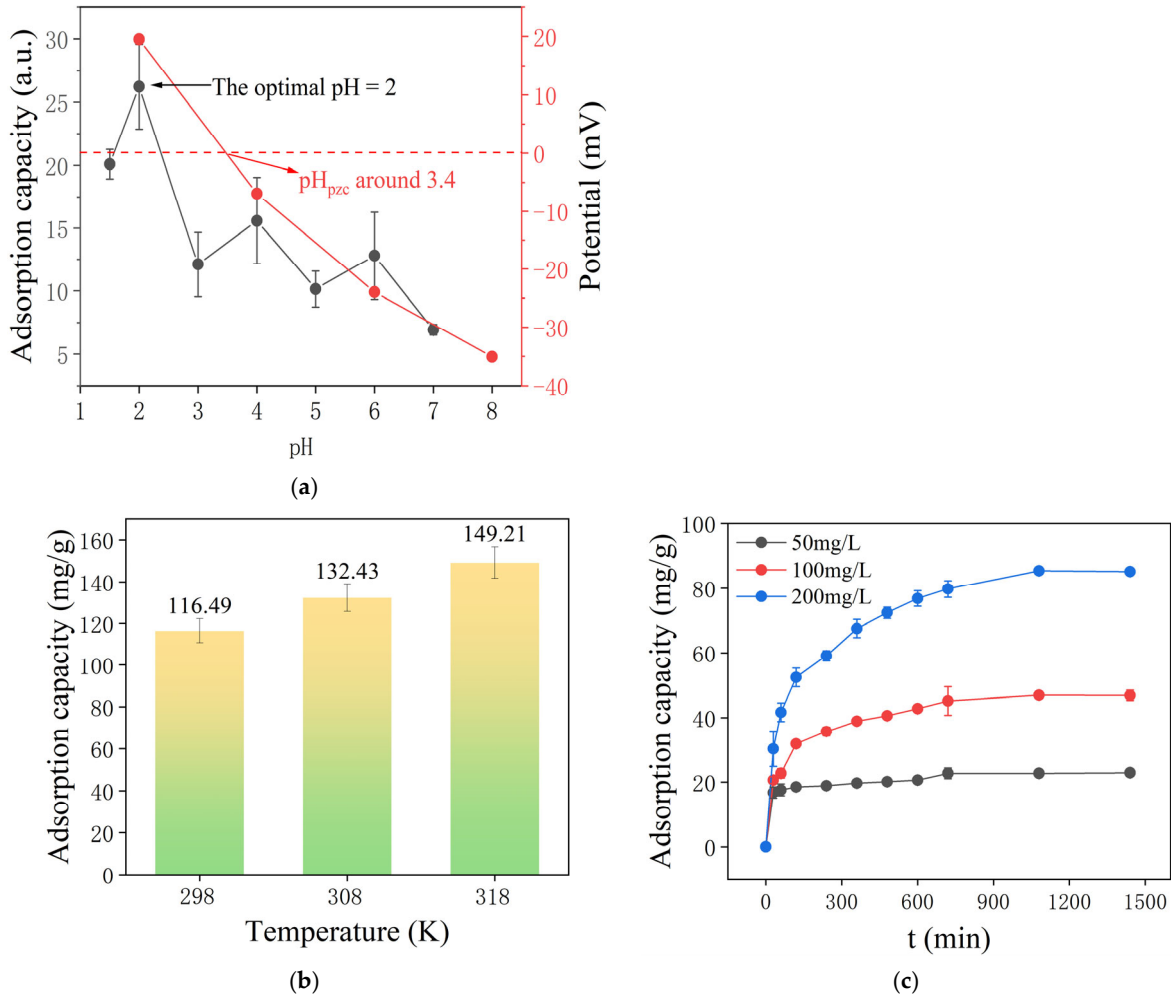

Figure 4. Cr(VI) sorptive characteristics of NS-HCS: (**a**) pH-dependent Cr(VI) sequestration (0.4 g/L adsorbent loading, pH 1.5–7 range, 50 mg/L Cr(VI) solutions, 24 h thermo-regulated agitation); (**b**) thermal effects on adsorption efficacy (0.4 g/L material dosage, pH 2 environment, 50 mg/L Cr(VI) concentration, 24 h equilibration); (**c**) concentration-dependent adsorption profiles (0.4 g/L NS-HCS loading, pH 2 conditions, variable Cr(VI) concentrations, 24 h constant-temperature oscillation).

Table 2. Theoretical maximum Cr(VI) adsorption capacities of various adsorbents.

Hydrothermal Carbon	q_{max}-Cr(VI) (mg/g)	Ref.
Tectona grandis tree using $ZnCl_2$	127.00	[40]
microalgae (*Chlorococcum* sp.) using NH_3	95.70	[41]
peanut hulls using HDA	142.86	[42]
Eucalyptus sawdust using KOH	45.88	[43]
NS-HCS	149.21	This study

Cr(VI) adsorption dynamics exhibited concentration-dependent escalation patterns, with NS-HCS demonstrating augmented sorptive performance at elevated Cr(VI) concentrations. This phenomenon arises from amplified interfacial collision probabilities between Cr(VI) oxyanions and active adsorption sites under higher solute loading conditions [44,45]. The electrochemical potential gradients between free Cr(VI) ions in bulk solution and surface-bound species enhanced interfacial accumulation kinetics [28]. Experimental protocols employed tripartite concentration gradients (50–200 mg/L) to assess NS-HCS's concentration responsiveness. Quantitative analysis revealed a progressive capacity intensification from 22.86 mg/g (50 mg/L) to 85.26 mg/g (200 mg/L), which

confirmed concentration-modulated adsorption efficacy (Figure 4c). This suggests that higher concentrations of the Cr(VI) solution are more favorable for the adsorption process by NS-HCS, as the greater potential energy difference between the solution and NS-HCS promotes the contact and capture of Cr(VI) by NS-HCS. Using identical concentration, the research further investigated how the duration of adsorption affects the adsorption capacity of NS-HCS. Typically, over time, the adsorption mechanism of the Cr(VI) adsorbent stabilizes. Before reaching equilibrium, the adsorption potential of the adsorbent remains underutilized. Therefore, identifying the point at which the adsorption process stabilizes is crucial for achieving peak capacity [16,29]. The findings revealed an increase in NS-HCS's ability to adsorb Cr(VI) over time, with the process continuing up to 1080 min, highlighting the importance of maintaining the interaction duration between NS-HCS and Cr(VI) at 1080 min for peak capacity.

3.3. Kinetic Models

Kinetic curves effectively reflect the adsorption performance and physicochemical interaction processes of adsorbents. This investigation employed PFO (pseudo-first-order) and PSO (pseudo-second-order) kinetic models to interpret Cr(VI)) uptake data across 0.5–24 h durations. Concentration-dependent kinetic trajectories (50–200 mg/L Cr(VI)) were analyzed to elucidate NS-HCS's Cr(VI) sequestration pathways and predict operational efficiency [37]. Results from the kinetic fitting revealed nearly identical kinetic curves across various concentrations, implying that concentration did not significantly affect the adsorption and equilibrium patterns of NS-HCS. NS-HCS's ability to adsorb Cr(VI) showed a rapid increase during the initial 120 min, followed by a gradual deceleration until it stabilized after 1080 min. This biphasic behavior originates from abundant surface binding sites, and initial Cr(VI) concentration gradients accelerated interfacial accumulation. Progressive site saturation and intraparticle diffusion requirements through porous matrices subsequently reduced adsorption rates. Concurrently, given the dynamic nature of adsorption-desorption, a segment of Cr(VI) is likely to be re-released once equilibrium is achieved (Figure 5a–c) [27]. Comparative model fitting demonstrated PSO superiority (R^2 = 0.961/0.978/0.978) over PFO (R^2 = 0.929/0.928/0.923), with PSO-derived equilibrium capacities aligning closely with experimental values. This suggests that the adsorption mechanism of NS-HCS for Cr(VI) is better described by the pseudo-second-order kinetic model, which assumes chemical adsorption as the controlling factor. This implies that the adsorption process is primarily influenced by the chemical interaction between NS-HCS and Cr(VI).

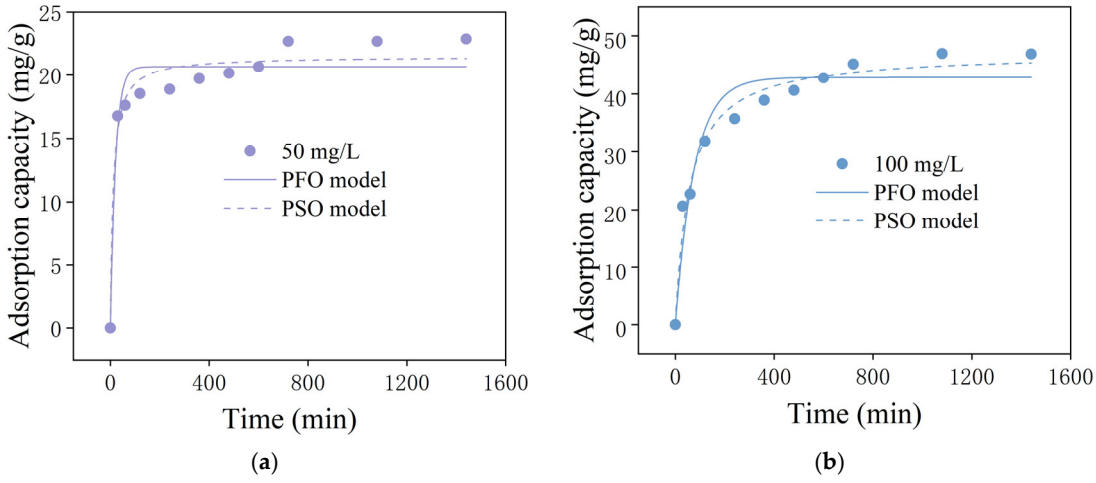

Figure 5. *Cont.*

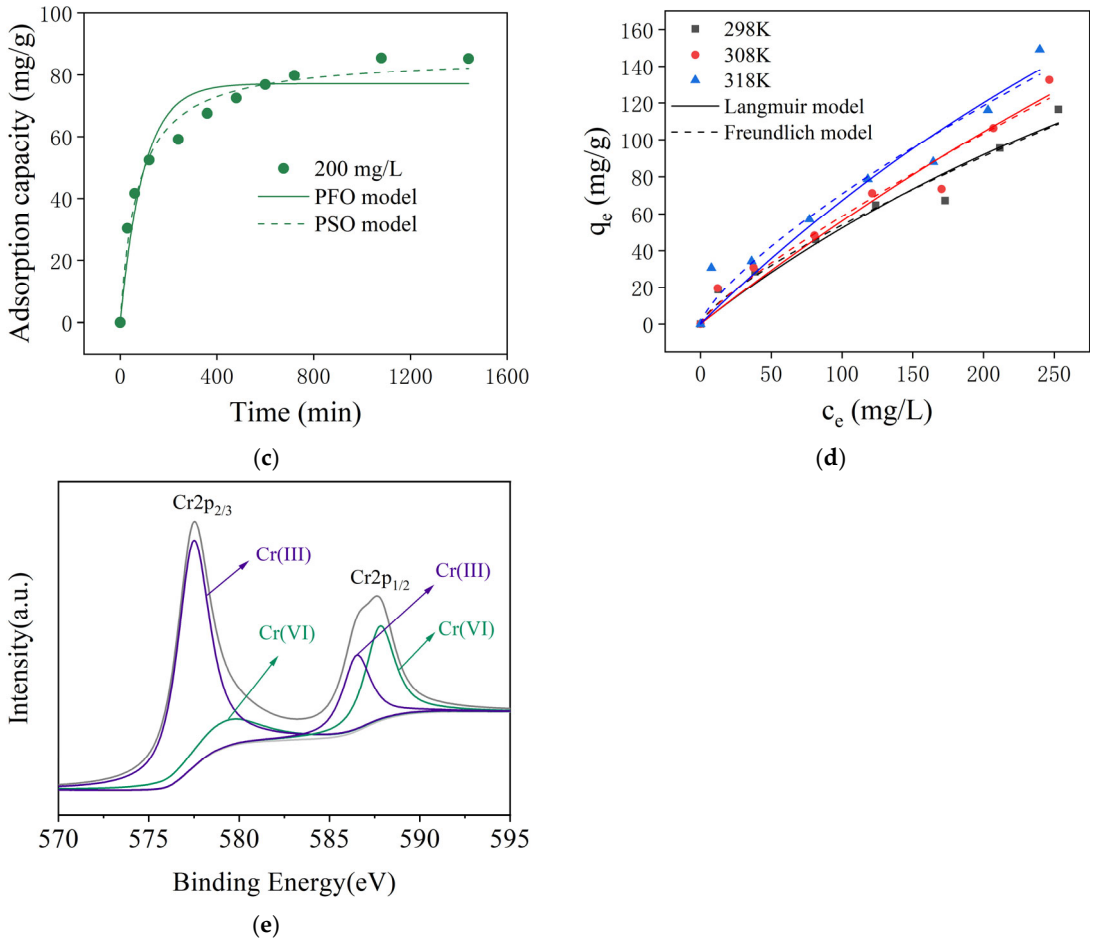

Figure 5. Cr(VI) sorption kinetic modeling for NS-HCS under varying concentrations (0.4 g/L adsorbent, pH 2): (**a**) 100 mg/L Cr(VI) solution; (**b**) 200 mg/L Cr(VI) solution; (**c**) 300 mg/L Cr(VI) solution; (**d**) isothermal equilibrium profiles; (**e**) post-sorption X-ray photoelectron spectroscopic analysis of Cr(VI)-laden NS-HCS.

3.4. Isotherms and Thermodynamics

The isothermal adsorption technique was employed to more effectively confirm NS-HCS's adsorption efficacy for Cr(VI), examining the chemical interaction between NS-HCS and Cr(VI). Analytical frameworks incorporating Langmuir (monolayer sorption) and Freundlich (multi-layered sorption) isotherm models were applied to interpret Cr(VI) distribution patterns [46]. Experimental protocols involved Cr(VI) solutions (from 20 to 300 mg/L) interacting with NS-HCS under thermal gradients (298, 308, and 318 K) during 24 h equilibrium periods. Freundlich model regression demonstrated enhanced correlation coefficients compared to Langmuir approximations, confirming multi-layered sorption predominance (Figure 5d). Post-adsorption XPS analysis of Cr(VI)-loaded NS-HCS revealed the predominant presence of Cr(III) over Cr(VI) on the material surface (Figure 5e). This observation suggests that nitrogen doping facilitated the reduction of Cr(VI) to Cr(III), followed by subsequent adsorption of the reduced Cr(III) species. The multilayer adsorption behavior likely involves a sequential process of Cr(VI) adsorption, reduction, and Cr(III) adsorption. This phenomenon can be attributed to the nitrogen functional groups (particularly pyridinic-N) introduced through the urea-assisted secondary hydrothermal treatment, which created active sites for both Cr(VI) adsorption and reduction.

Thermodynamic evaluations elucidate energetic transformations inherent in Cr(VI) adsorption mechanisms. Experimental determinations quantified Gibbs free energy (ΔG°), enthalpy (ΔH°), and entropy (ΔS°) variations across thermal gradients (Table 3). The findings

revealed negative values for both ΔG° and ΔH° at three different temperatures, with a ΔH° of −7.43 kJ/mol, suggesting that the adsorption mechanism operates on exothermic principles. The presence of negative ΔG° values indicates that the adsorption occurs naturally, without the need for external energy [47]. The ΔS° positivity reflects enhanced molecular disorder at sorption interfaces, aligning with entropy-governed adsorption pathways.

Table 3. Thermodynamic parameters of adsorption of Cr(VI) by NS-HCS.

T (K)	ΔG° (kJ/mol)	ΔH° (kJ/mol)	ΔS° (kJ/(K/mol))
298	−10.97		
308	−9.64	−7.43	0.01
318	−11.24		

3.5. Ion Competition and Regeneration

During the real-world use of Cr(VI) for treating wastewater, various ions in the mixture often compete with Cr(VI) for absorption sites. This research used K^+, Ca^{2+}, Mg^{2+}, PO_4^{3-}, CO_3^{2-}, SO_4^{2-}, and Cl^- as experimental ions that were present alongside Cr(VI). The adsorption experiments were conducted using NS-HCS at a temperature of 25 °C over a 24 h period, maintaining a Cr(VI) solution at a concentration of 50 mg/L. The findings revealed that the presence of K^+, Ca^{2+}, Mg^{2+}, and Cl^- had minimal impact on Cr(VI) adsorption, suggesting that the active sites for Cr(VI) adsorption on NS-HCS surfaces do not interact with these ions. Under acidic conditions, Cr(VI) primarily exists as $HCrO_4^-$ ions (Figure 6a). When the pH is below 3.4, the surface of NS-HCS carries a positive charge, allowing for electrostatic adsorption with Cr(VI) [35,38,39]. Nonetheless, the presence of PO_4^{3-}, CO_3^{2-}, and SO_4^{2-} hindered the binding of Cr(VI) to the active sites on NS-HCS. However, in these cases, NS-HCS's ability to adsorb Cr(VI) remained above 50%, indicating its specific affinity for Cr(VI) adsorption.

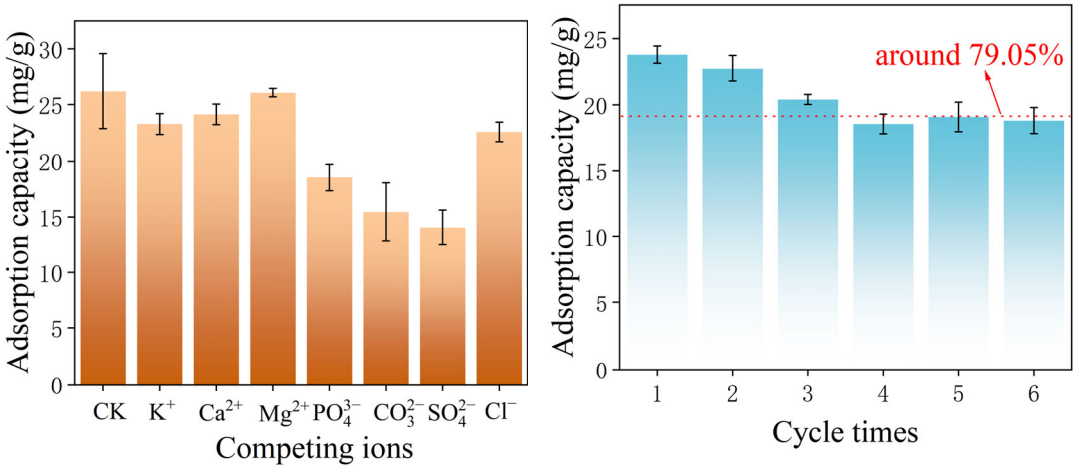

Figure 6. Evaluation of the application potential of NS-HCS (dosage: 0.4 g/L, pH = 2, Cr(VI) concentration: 50 mg/L): (**a**) multi-ionic interference simulation; (**b**) cyclic adsorption–regeneration durability testing.

The ability of an adsorbent to regenerate is vital, as it directly impacts its economic value and ecological benefits. The changes in the adsorption performance of NS-HCS were recorded over multiple cycles of use. After the first four cycles, a reduction in NS-HCS's adsorption capacity was observed, possibly due to alterations in its physical composition or chemical properties during these cycles [48–50]. However, after the fourth cycle, NS-HCS

maintained an adsorption capacity of approximately 79.05% for Cr(VI), indicating that it continued to show remarkable stability and the ability to regenerate Cr(VI) adsorption, even after an initial decline in performance (Figure 6b) [51]. In summary, NS-HCS showed an effective adsorption of Cr(VI) in wastewater, sustaining its adsorption efficiency even after multiple uses, underscoring its practical applicability.

3.6. Actual Water Treatment Experiment

A real-world applicability assessment of NS-HCS employed Chaohu Lake water, Fei River samples, precipitation runoff, and municipal tap water as adsorption matrices, each spiked with 50 mg L^{-1} Cr(VI) [33]. Adsorption trials conducted under controlled conditions (25 °C, 24 h equilibrium) with 0.4 g L^{-1} NS-HCS dosage demonstrated exceptional Cr(VI) retention across all aqueous matrices. Comparative analysis against ultrapure water references revealed sustained adsorption efficiencies exceeding 90% retention rates (Figure 7).

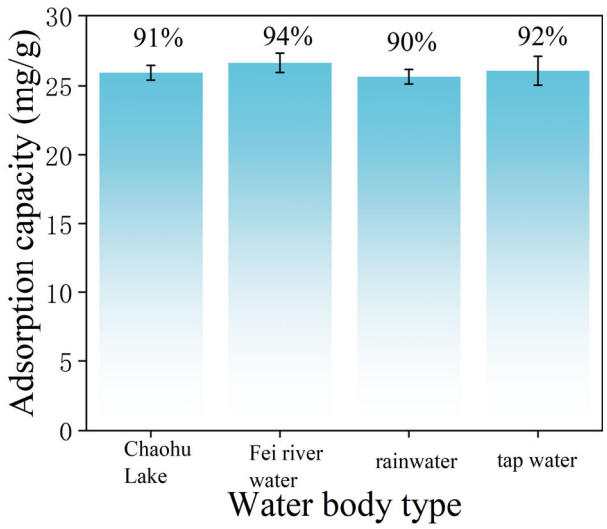

Figure 7. Practical implementation assessment of NS-HCS (0.4 g/L material loading, pH 2 environment, 50 mg/L Cr(VI) solutions): natural aqueous matrix performance validation.

These empirical findings validate ion competition experimental conclusions while demonstrating viability for practical wastewater remediation applications. This discovery offers a novel strategy for designing high-performance adsorbents with dual advantages of efficiency and environmental sustainability.

4. Conclusions

This study successfully synthesized nitrogen-doped starch-based hydrothermal carbon (NS-HCS) from starch using a two-step hydrothermal method, effectively enhancing its adsorption capacity for Cr(VI) in wastewater. The findings indicated that NS-HCS demonstrated superior adsorption capabilities, reaching 149.21 mg/g. In-depth analysis revealed that NS-HCS possesses an extensive specific surface area and numerous oxygen-rich functional groups. After nitrogen doping and secondary hydrothermal treatment, significant changes were observed in ν-OH, C-H, C=O, ν-C=C, and C-OH, indicating that nitrogen doping affected these functional groups, which, in turn, enhanced the adsorption capacity for Cr(VI). Experiments involving recycling and competitive adsorption revealed that NS-HCS exhibits effective regeneration and resistance to interference, making it suitable for real-world applications. To summarize, NS-HCS stands out as a potent and ecofriendly material for extracting Cr(VI) from aqueous solutions, offering a feasible alternative to

conventional adsorbents, particularly in industrial settings with significant Cr(VI) contamination. The research introduces an innovative, ecofriendly method for addressing Cr(VI)-polluted industrial wastewater.

Supplementary Materials: The following supporting information can be downloaded at: https://www.mdpi.com/article/10.3390/su17114982/s1.

Author Contributions: All authors have contributed to all aspects of the article. All authors have read and agreed to the published version of the manuscript.

Funding: This research was funded by the National Key Research and Development Program of China, grant numbers 2018YFD0800203 and 2023YFD1702103.

Institutional Review Board Statement: Not applicable.

Informed Consent Statement: Not applicable.

Data Availability Statement: The data presented in this study are available upon request from the corresponding author.

Acknowledgments: We appreciate the anonymous reviewers for their invaluable comments and suggestions on this manuscript.

Conflicts of Interest: The authors declare no conflicts of interest.

Abbreviations

The following abbreviations are used in this manuscript:

NS-HCS	Nitrogen-doped starch-based hydrothermal carbon
SHCS	Starch-based hydrothermal carbon

References

1. Xie, S. Water contamination due to hexavalent chromium and its health impacts: Exploring green technology for Cr (VI) remediation. *Green Chem. Lett. Rev.* **2024**, *17*, 2356614. [CrossRef]
2. He, G.; Xiao, Y.; Du, H. An overview and recent progress in photocatalytic Cr (VI) reduction and hydrogen evolution. *Int. J. Hydrogen Energy* **2024**, *53*, 633–646. [CrossRef]
3. Fan, X.; Xin, R.; Li, L.; Zhang, B.; Li, C.; Zhou, X.; Chen, H.; Zhang, H.; OuYang, F.; Zhou, Y. Progress in the preparation and physical properties of two-dimensional Cr-based chalcogenide materials and heterojunctions. *Front. Phys.* **2024**, *19*, 23401. [CrossRef]
4. Huang, H.; Gao, Y.-J.; Cao, Z.-X.; Tian, Z.-Q.; Bai, Y.-F.; Tang, Z.-X.; Ali, A.; Zhao, F.-J.; Wang, P. Ecotoxicity of hexavalent chromium [Cr (VI)] in soil presents predominate threats to agricultural production with the increase of soil Cr contamination. *J. Hazard. Mater.* **2024**, *476*, 135091. [CrossRef]
5. Koc, I.; Cobanoglu, H.; Canturk, U.; Key, K.; Kulac, S.; Sevik, H. Change of Cr concentration from past to present in areas with elevated air pollution. *Int. J. Environ. Sci. Technol.* **2024**, *21*, 2059–2070. [CrossRef]
6. Min, X.; Zhang, K.; Chen, J.; Chai, L.; Lin, Z.; Zou, L.; Liu, W.; Ding, C.; Shi, Y. Bacteria-driven copper redox reaction coupled electron transfer from Cr (VI) to Cr (III): A new and alternate mechanism of Cr (VI) bioreduction. *J. Hazard. Mater.* **2024**, *461*, 132485. [CrossRef]
7. Keshta, B.E.; Yu, H.; Wang, L.; Gemeay, A.H. Cutting-edge in the green synthesis of MIL-101 (Cr) MOF based on organic and inorganic waste recycling with extraordinary removal for anionic dye. *Sep. Purif. Technol.* **2024**, *332*, 125744. [CrossRef]
8. Cheng, S.; Zeng, X.; Liu, P. One-step synthesis of magnetic N-doped carbon nanotubes derived from waste plastics for effective Cr (VI) removal. *Arab. J. Chem.* **2024**, *17*, 105956. [CrossRef]
9. Verma, B.; Balomajumder, C. Magnetic magnesium ferrite–doped multi-walled carbon nanotubes: An advanced treatment of chromium-containing wastewater. *Environ. Sci. Pollut. Res.* **2020**, *27*, 13844–13854. [CrossRef]
10. Zhong, G.; Huang, J.; Yao, Z.; Luo, B.; Li, K.; Xu, S.; Fu, X.; Cao, Y. Intrinsic acid resistance and high removal performance from the incorporation of nickel nanoparticles into nitrogen doped tubular carbons for environmental remediation. *J. Colloid Interface Sci.* **2020**, *566*, 46–59. [CrossRef]

11. Song, Z.; Xu, Y.; Zhang, M.; Zhu, W.; Yang, X.; Hao, D.; Li, Q. Efficient removal of Cr (VI) by Bifunction zinc porphyrin COF: Coupling adsorption with Photocatalysis, performance Evaluation, and mechanism analysis. *J. Colloid Interface Sci.* **2025**, *677*, 346–358. [CrossRef] [PubMed]
12. Wang, C.; You, C.; Rong, K.; Shen, C.; Yang, F.; Li, S. An S-scheme MIL-101 (Fe)-on-BiOCl heterostructure with oxygen vacancies for boosting photocatalytic removal of Cr (VI). *Acta Phys.-Chim. Sin.* **2024**, *40*, 2307045. [CrossRef]
13. Fan, Y.; Olsson, E.; Johannessen, B.; D'angelo, A.M.; Thomsen, L.; Cowie, B.; Smillie, L.; Liang, G.; Lei, Y.; Bo, G.; et al. Manipulation of transition metal migration via cr-doping for better-performance li-rich, co-free cathodes. *ACS Energy Lett.* **2024**, *9*, 487–496. [CrossRef]
14. Bogireddy, N.K.R.; Rios, S.E.S.; Agarwal, V. Simple one step synthesis of dual-emissive heteroatom doped carbon dots for acetone sensing in commercial products and Cr (VI) reduction. *Chem. Eng. J.* **2021**, *414*, 128830. [CrossRef]
15. Qin, X.; Tao, R.; Cheng, S.; Xing, B.; Meng, W.; Nie, Y.; Zhang, C.; Yu, J. Microwave-assisted one-pot method preparation of ZnO decorated biochar for levofloxacin and Cr (VI) removal from wastewater. *Ind. Crops Prod.* **2024**, *208*, 117863. [CrossRef]
16. Yazid, H.; Bouzid, T.; El Mouchtari, E.M.; Bahsis, L.; El Himri, M.; Rafqah, S.; El haddad, M. Insights into the adsorption of Cr (VI) on activated carbon prepared from walnut shells: Combining response surface methodology with computational calculation. *Clean Technol.* **2024**, *6*, 199–220. [CrossRef]
17. Chen, Y.; Qian, Y.; Ma, J.; Mao, M.; Qian, L.; An, D. New insights into the cooperative adsorption behavior of Cr (VI) and humic acid in water by powdered activated carbon. *Sci. Total Environ.* **2022**, *817*, 153081. [CrossRef]
18. Du, H.; Yuan, D.; Li, W.; Wang, L.; Li, Y.; Che, L.; Tian, W.; Salama, E.; Ossman, M.; Lin, F. Efficient removal of toxic organics and reduction of Cr (VI) to Cr (III) from tannery sludge: A comparative study of microwave pyrolysis and conventional pyrolysis. *Sep. Purif. Technol.* **2025**, *354*, 128736. [CrossRef]
19. Li, S.; Dong, K.; Cai, M.; Li, X.; Chen, X. A plasmonic S-scheme Au/MIL-101 (Fe)/BiOBr photocatalyst for efficient synchronous decontamination of Cr (VI) and norfloxacin antibiotic. *EScience* **2024**, *4*, 100208. [CrossRef]
20. Sujatha, S.; Sivarethinamohan, R. A critical review of Cr (VI) ion effect on mankind and its amputation through adsorption by activated carbon. *Mater. Today Proc.* **2021**, *37*, 1158–1162. [CrossRef]
21. Jawed, A.; Golder, A.K.; Pandey, L.M. Bio-based iron oxide nanoparticles forming bi-functional chitosan composite adsorbent for Cr (VI) decontamination. *Chem. Eng. J.* **2024**, *481*, 148411. [CrossRef]
22. Liang, H.; Zhang, H.; Zhao, P.; Zhao, X.; Sun, H.; Geng, Z.; She, D. Synthesis of a novel three-dimensional porous carbon material and its highly selective Cr (VI) removal in wastewater. *J. Clean. Prod.* **2021**, *306*, 127204. [CrossRef]
23. Cao, D.; Guan, J.; Du, J.; Sun, Q.; Ma, J.; Li, J.; Liu, J.; Sheng, G. Halogen-functionalized covalent organic frameworks for photocatalytic Cr (VI) reduction under visible light. *J. Hazard. Mater.* **2024**, *476*, 134956. [CrossRef]
24. Hasija, V.; Raizada, P.; Singh, P.; Verma, N.; Khan, A.A.P.; Singh, A.; Selvasembian, R.; Kim, S.Y.; Hussain, C.M.; Nguyen, V.-H.; et al. Progress on the photocatalytic reduction of hexavalent Cr (VI) using engineered graphitic carbon nitride. *Process Saf. Environ. Prot.* **2021**, *152*, 663–678. [CrossRef]
25. Wang, K.; Zeng, S.; Li, G.; Dong, Y.; Wang, Q.; Zhang, L.; Ren, Z.; Wang, P. Superoxide radical induced redox processes for simultaneous reduction of Cr (VI) and oxidation of ciprofloxacin in wastewater. *Appl. Catal. B Environ.* **2024**, *343*, 123565. [CrossRef]
26. Li, K.; Xu, W.; Song, H.; Bi, F.; Li, Y.; Jiang, Z.; Tao, Y.; Qu, J.; Zhang, Y. Superior reduction and immobilization of Cr (VI) in soil utilizing sulfide nanoscale zero-valent iron supported by phosphoric acid-modified biochar: Efficiency and mechanism investigation. *Sci. Total Environ.* **2024**, *907*, 168133. [CrossRef]
27. Song, J.; Meng, Z.; Wang, X.; Zhang, G.; Bi, C.; Hou, J. One-step microwave method synthesis of Fe_3O_4 nanoribbon@ carbon composite for Cr (VI) removal. *Sep. Purif. Technol.* **2022**, *298*, 121530. [CrossRef]
28. Mazkad, D.; El Idrissi, A.; Marrane, S.E.; Lazar, N.E.; El Ouardi, M.; Dardari, O.; Channab, B.E.; Ait Layachi, O.; Farsad, S.; Baqais, A.; et al. An innovative diatomite-polypyrrole composite for highly efficient Cr (VI) removal through optimized adsorption via surface response methodology. *Colloids Surf. A Physicochem. Eng. Asp.* **2024**, *685*, 133172. [CrossRef]
29. Asimakopoulos, G.; Baikousi, M.; Salmas, C.; Bourlinos, A.B.; Zboril, R.; Karakassides, M.A. Advanced Cr (VI) sorption properties of activated carbon produced via pyrolysis of the "*Posidonia oceanica*" seagrass. *J. Hazard. Mater.* **2021**, *405*, 124274. [CrossRef]
30. Juturu, R.; Murty, V.R.; Selvaraj, R. Efficient adsorption of Cr (VI) onto hematite nanoparticles: ANN, ANFIS modelling, isotherm, kinetic, thermodynamic studies and mechanistic insights. *Chemosphere* **2024**, *349*, 140731. [CrossRef]
31. Poudel, M.B.; Awasthi, G.P.; Kim, H.J. Novel insight into the adsorption of Cr (VI) and Pb (II) ions by MOF derived Co-Al layered double hydroxide@ hematite nanorods on 3D porous carbon nanofiber network. *Chem. Eng. J.* **2021**, *417*, 129312. [CrossRef]
32. Wang, M.; Chen, Y.; Zhang, Y.; Wei, S.; Zhao, X.; Zhao, K.; Xu, L.; Feng, X. Selective removal of Cr (VI) from solution by polyethyleneimine modified hydrochar loaded nanoscale zero-valent iron with high adsorption capacity. *Sep. Purif. Technol.* **2024**, *329*, 125150. [CrossRef]
33. Fang, W.; Wu, H.; Ma, K.; Zuo, B.; She, D.; Geng, Z.; Liang, H. Efficient selective adsorption of Cr (VI) by S-doped porous carbon prepared from industrial lignin: Waste increment and wastewater treatment. *Int. J. Biol. Macromol.* **2024**, *278*, 134765. [CrossRef]

34. Wang, L.; Sha, Y.; Bi, C.; Lin, D.; Liu, Y.; Dai, L.; Wang, X.; Lin, H.; Jrar, J.A.; Hou, J. One-step microwave method synthesis of N, S-codoped carbon with the frustrated Lewis pairs for Cr (VI) removal. *J. Water Process Eng.* **2025**, *69*, 106757. [CrossRef]
35. Shen, Y.; Ma, Y.; Zhang, C.; Wang, Y.; Wang, H.; Li, P. Simultaneous excellent catalytic performances toward hydrogenation reduction of 4-nitrophenol and reduction of Cr (VI) in water by novel designing of Cu-CoO/N-doped carbon nanocatalysts. *Appl. Surf. Sci.* **2024**, *644*, 158780. [CrossRef]
36. Zeng, L.; Zhu, Y.; Wu, D.; Cheng, H.; Zhou, Q. Cr selectively incorporated N, S-doped carbon layer encapsulating Ir/IrO_2 for efficient alkaline hydrogen and oxygen evolution. *J. Alloys Compd.* **2025**, *1010*, 177371. [CrossRef]
37. Al Lafi, A.G.; Khuder, A. Removal of Cr (VI) from aqueous solutions by activated carbon and its composite with P2W17O61: A spectroscopic study to reveal adsorption mechanism. *Heliyon* **2025**, *11*, e41862. [CrossRef]
38. Guo, Y.; Chen, M.; Gao, T.; Lin, J.; Zhang, J.; Chen, T.; Guo, Y.; Hua, S. Interaction and band structure-determined inhibition of negative Cr (VI) and positive Fe (III) for antibiotic photodegradation by nitrogen-doped dissolved black carbon. *Chemosphere* **2024**, *364*, 143234. [CrossRef]
39. Hakim, M.; Faruk, S.; Kabir, M.M.; Chowdhury, F.; Ahmed, F.; Khan, A.A.; Islam, D.; Lipy, E.P.; Akhter, S. Agro-waste-based functionalized mesoporous activated carbon for the effective remediation of Cr (VI) from wastewater. *Biomass Convers. Biorefinery* **2024**, 1–15. [CrossRef]
40. Vo, A.T.; Nguyen, V.P.; Ouakouak, A.; Nieva, A.; Doma, B.T., Jr.; Tran, H.N.; Chao, H.-P. Efficient Removal of Cr(VI) from Water by Biochar and Activated Carbon Prepared through Hydrothermal Carbonization and Pyrolysis: Adsorption-Coupled Reduction Mechanism. *Water* **2019**, *11*, 1164. [CrossRef]
41. Sun, Y.; Liu, C.; Zan, Y.; Miao, G.; Wang, H.; Kong, L. Hydrothermal carbonization of microalgae (*Chlorococcum* sp.) for porous carbons with high Cr (VI) adsorption performance. *Appl. Biochem. Biotechnol.* **2018**, *186*, 414–424. [CrossRef] [PubMed]
42. Cai, W.; Wei, J.; Li, Z.; Liu, Y.; Zhou, J.; Han, B. Preparation of amino-functionalized magnetic biochar with excellent adsorption performance for Cr (VI) by a mild one-step hydrothermal method from peanut hull. *Colloids Surf. A Physicochem. Eng. Asp.* **2019**, *563*, 102–111. [CrossRef]
43. Zhang, X.; Zhang, L.; Li, A. Eucalyptus sawdust derived biochar generated by combining the hydrothermal carboni-zation and low concentration KOH modification for hexavalent chromium removal. *J. Environ. Manag.* **2018**, *206*, 989–998. [CrossRef]
44. Kleinberg, M.N.; Thamaraiselvan, C.; Powell, C.D.; Ronen, A.; Arnusch, C.J. Reduction of Cr (VI) to Cr (III) by activated carbon cloth through adsorption and electrochemical processes. *ACS Appl. Eng. Mater.* **2023**, *1*, 901–912. [CrossRef]
45. Kaur, J.; Kaur, M.; Ubhi, M.K.; Kaur, N.; Greneche, J.M. Composition optimization of activated carbon-iron oxide nanocomposite for effective removal of Cr (VI) ions. *Mater. Chem. Phys.* **2021**, *258*, 124002. [CrossRef]
46. Wang, Y.; Wen, S.; Guo, J.; Gao, Y.; Xu, Y.; Xue, W. Sulfidized nanoiron-loaded carbon for efficient removal of Cr (VI) from wastewater. *Mater. Chem. Phys.* **2024**, *327*, 129918. [CrossRef]
47. Xie, J.; Wei, K.; Liu, X.; Fang, D. Effect of carbon type on the detoxification mechanism of hexavalent chromium [Cr (VI)] by carbothermal reduction. *J. Environ. Chem. Eng.* **2022**, *10*, 108091. [CrossRef]
48. Chen, H.; Zhang, Z.; Zhong, X.; Zhuo, Z.; Tian, S.; Fu, S.; Chen, Y.; Liu, Y. Constructing MoS2/Lignin-derived carbon nanocomposites for highly efficient removal of Cr (VI) from aqueous environment. *J. Hazard. Mater.* **2021**, *408*, 124847. [CrossRef]
49. Chen, X.; Song, Z.; Yuan, B.; Li, X.; Li, S.; Nguyen, T.T.; Guo, M.; Guo, Z. Fluorescent carbon dots crosslinked cellulose Nanofibril/Chitosan interpenetrating hydrogel system for sensitive detection and efficient adsorption of Cu (II) and Cr (VI). *Chem. Eng. J.* **2022**, *430*, 133154. [CrossRef]
50. Yuan, H.; Peng, J.; Ren, T.; Luo, Q.; Luo, Y.; Zhang, N.; Huang, Y.; Guo, X.; Wu, Y. Novel fluorescent lignin-based hydrogel with cellulose nanofibers and carbon dots for highly efficient adsorption and detection of Cr (VI). *Sci. Total Environ.* **2021**, *760*, 143395. [CrossRef]
51. Li, J.; Cheng, R.; Chen, J.; Lan, J.; Li, S.; Zhou, M.; Zeng, T.; Hou, H. Microscopic mechanism about the selective adsorption of Cr (VI) from salt solution on nitrogen-doped carbon aerogel microsphere pyrolysis products. *Sci. Total Environ.* **2021**, *798*, 149331. [CrossRef]